Supplemental Information

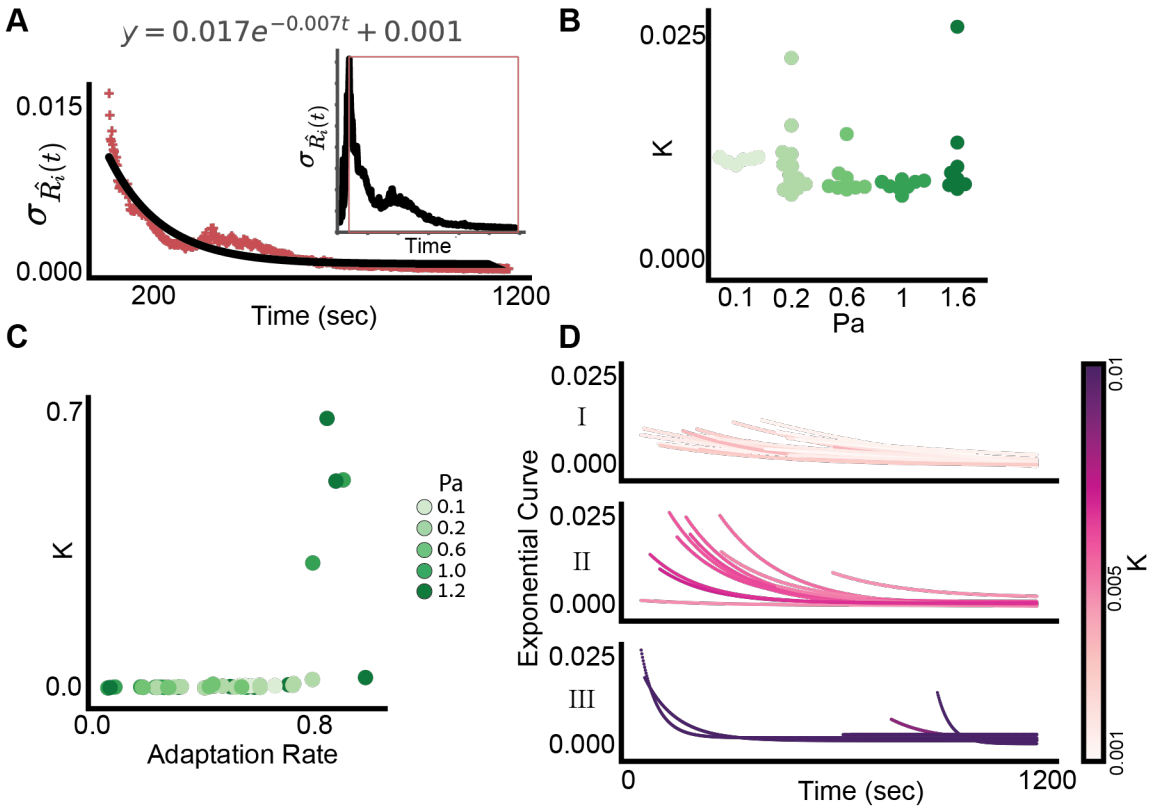

Figure S1: Parametric exponential model for multicellular calcium adaption.
(**A**) Fitting an exponential model A*e^-Kt + c (black) to experimental multicellular calcium dynamics (red '+' markers). Inset: calcium dynamics throughout the full experiment, the exponential fit considered the temporal range from the maximal signal until the end of the experiment (orange rectangle, Methods).
(**B**) The exponential model coefficient K for each pressure level. Each data point reports the K coefficient of the model fit for a single experiment. 4/47 experiments with K > 0.1 were excluded for visualization purposes.
(**C**) Correlation between the adaptation rate and K. N = 47 experiments pooled across all shear stress levels, Pearson correlation = 0.5160, p-value = 0.0002. Pearson correlation = 0.7140, p-value ≤ 0.0001 when excluding the 4 outlier experiments where the data did not fit the exponential model (K > 0.1).
(**D**) Exponential curves fitted for the N = 46 experiments across all shear stress levels. Color code (linear) encodes the K coefficient of the corresponding exponential fit. The curves were partitioned to 3 sub-panels for visualization purposes: (I) K < 0.004, (II) 0.004 ≤ K < 0.008 (III) K ≥ 0.008. One experiment was filtered (because the coefficient A was < 0).

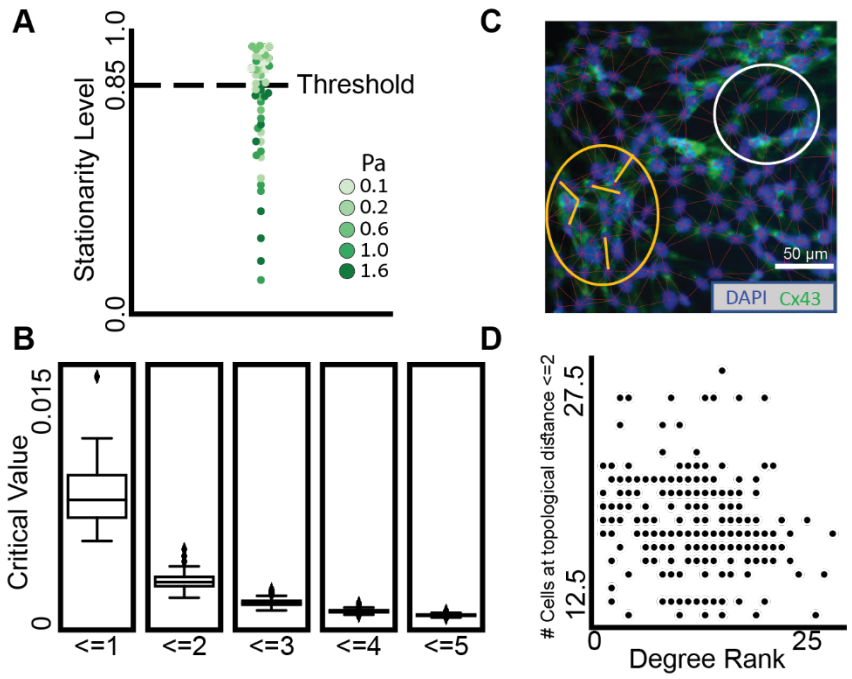

Figure S2: Stationarity and using topological distances of up to two in calculating the transmission and receiver score.

(A) Fraction of cells passing stationarity test per experiment. Each observation represents a biological replica. N = 47 biological replicates: n = 6 (0.1 Pa), n = 13 (0.2 Pa), n = 8 (0.6 Pa), n = 10 (1 Pa), n = 10 (1.6 Pa). In 23/47 experiments at least 85% of the cells passed both the KPSS and the ADF stationary tests with statistical significance levels below 0.05 (see Methods).

(B) Topological distance of two is a sweet spot in terms of reducing the false-positive errors (representative of ten experiments). Critical value range after Bonferroni correction for each topological distance upper bound (see Methods for details).

(C) Topological distance of two to reduce the effect of irregular shapes of the cells. Typical immunofluorescent image with dual labeling of cell nucleus (DAPI, blue) and gap junction proteins (Cx43, green). The thin red lines connect nuclei of nearest neighbor cells (defined with Delaunay Triangulation). In the low density region (e.g., white circle), gap junctions only appear between nearest neighbors. In the high density region (e.g., orange circle), gap junctions also connect cells that are next-to-nearest neighbors (see example pairs indicated by orange lines). Our shear-stress experiments were mostly high cell density, with confluence greater than 85%. Our shear-stress experiments were mostly high cell density, with confluence greater than 85%.

(D) The number of neighbors at topological distance ≤ 2 have weak correlation with the degree rank (accumulation of in-degree and out-degree edges). N = 295 cells from one experiment (representative of ten experiments). Pearson coefficient = -0.1678, p-value =0.0039.

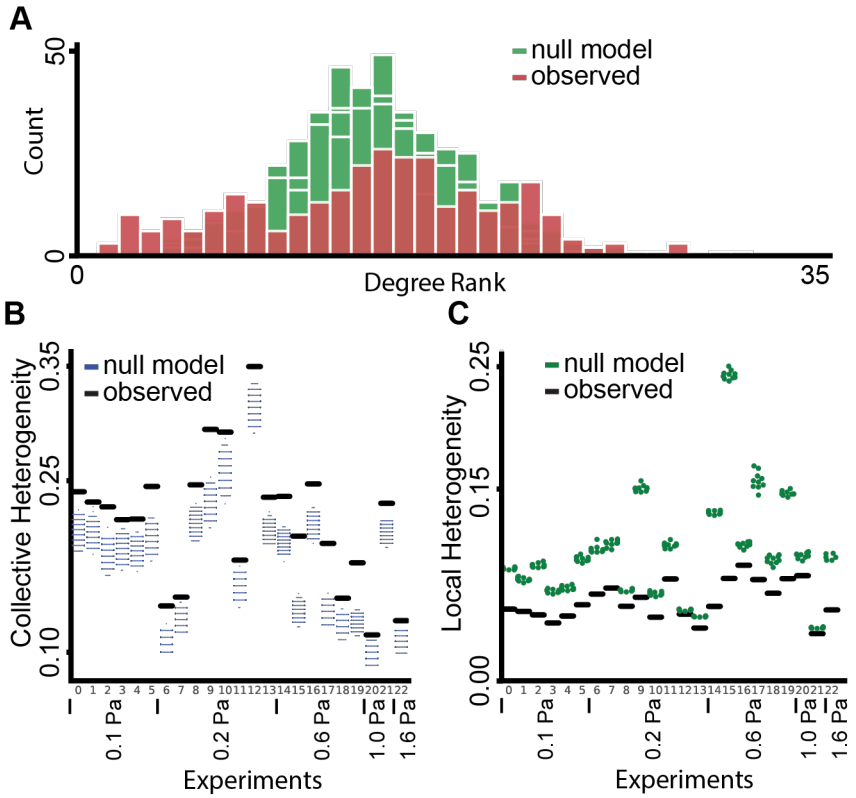

Figure S3: The multicellular network was characterized by collective heterogeneity and local homogeneity in its degree ranks.
(**A**) The degree rank distribution of n = 10 null model simulations (green, see Methods) and the observed network (red). The mean collective heterogeneity score as measured with (Jacob et al., 2017) (~0.29) is higher than the mean heterogeneity in the null models that considered random shuffling of GC edges while preserving the probability for an edge (~ 0.25, Methods). Representative of ten experiments.
(**B**) Collective heterogeneity across experiments. Observed collective heterogeneity (black) was higher than the null model (blue). N = 23 biological replicates, across shear stress levels, that passed the stationarity criterion.
(**C**) Local heterogeneity (Estrada's index (Estrada, 2010)) across experiments. Observed local heterogeneity (black) was lower (more homogeneous) than the null model (green) that rewired the edges while preserving the degree distribution of the original network. N = 23 biological replicates, across shear stress levels, that passed the stationarity criterion.

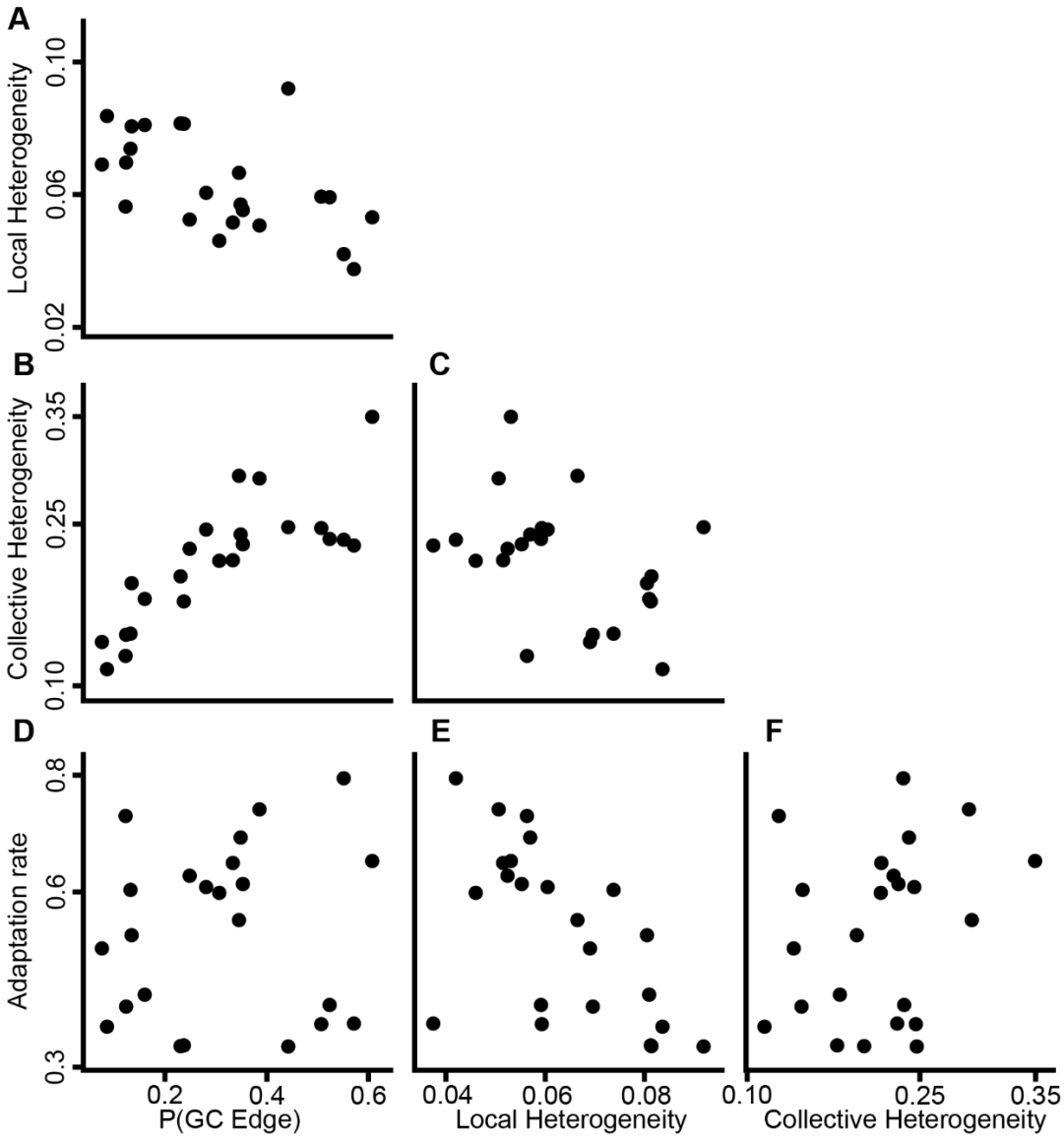

Figure S4: Correlating four measurements across experiments: multicellular adaptation, information flow, collective and local heterogeneity. N = 23 biological replicates, across shear stress levels, that passed the stationarity criterion were considered to calculate correlations.
(**A**) Local heterogeneity versus P(GC Edge). Pearson correlation = 0.55, p-value = 0.006.
(**B**) Collective heterogeneity versus P(GC edge). Pearson correlation = 0.80, p-value =0.000.
(**C**) Adaptation rate versus P(GC edge). Pearson correlation = 0.11, p-value = 0.615.
(**D**) Collective heterogeneity versus local heterogeneity. Pearson correlation = -0.41, p-value = 0.052.
(**E**) Adaptation rate versus local heterogeneity. Pearson correlation = -0.61, p-value = 0.002.
(**F**) Adaptation rate versus collective heterogeneity. Pearson correlation = 0.28, p-value =0.200.
Collective heterogeneity was correlated with the GC edge probability while the local heterogeneity was negatively associated with the adaptation rate as well as with the GC edge probability (and statistically marginally with the collective degree heterogeneity). The remaining measurement pair correlations were not statistically significant, but showed consistency in the correlation sign associating adaptation rate, GC edge probability, collective heterogeneity, and local homogeneity. One reason for the lack of statistical power could be the variability between experiments, including the varying shear stress magnitudes.

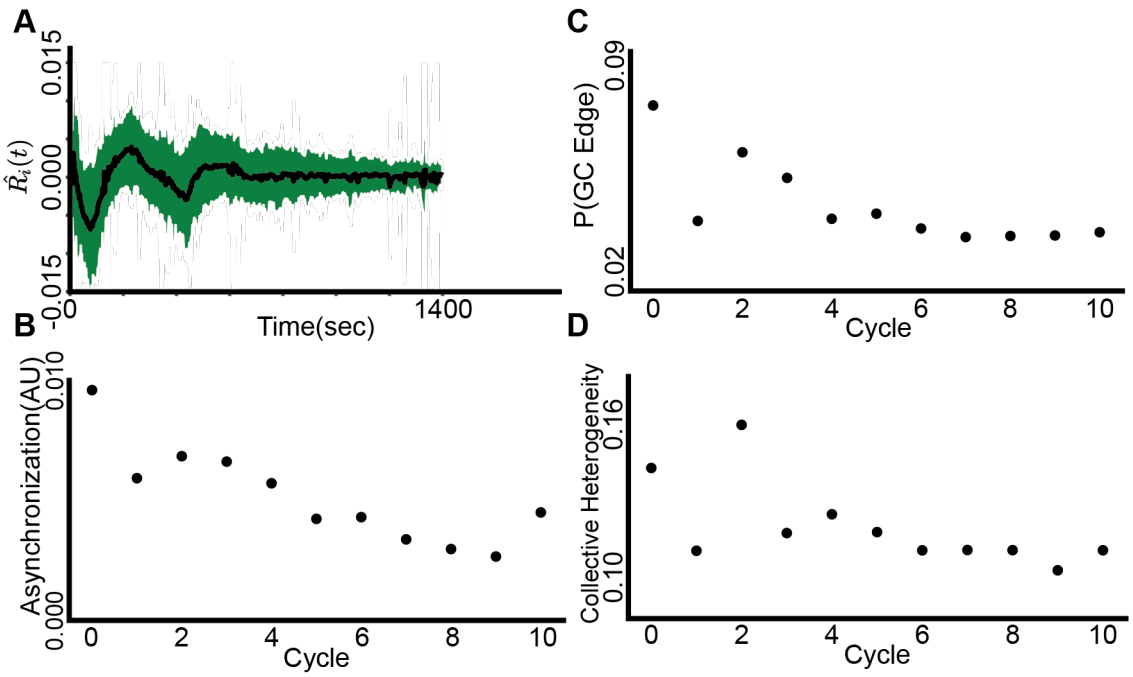

Figure S5: Sufficient cell density is required for multicellular synchronization. Shown are results for an experiment with sparse cell seeding. Representative of two experiments.
(**A**) Multicellular calcium dynamics over time in response to external mechanical stimuli. The calcium dynamics of each cell was represented by the time-derivative of its relative fluorescent intensity. Black: mean calcium *Ri*(*t*) dynamics; Green: standard deviation.
(**B**) Multicellular calcium dynamics synchronized over time for sparsely seeded cells. Pearson correlation = -0.8563, p-value = 0.0007. However, synchronization was less effective than in our baseline density experiments (compare to Fig. 3B and full results in Table S2).
(**C**) Information flow did not increase over time for sparsely seeded cells. Pearson correlation = -0.7581, p-value = 0.0068.
(**D**) Collective heterogeneity did not increase over time for sparsely seeded cells. Pearson correlation = -0.6517, p-value = 0.0298.

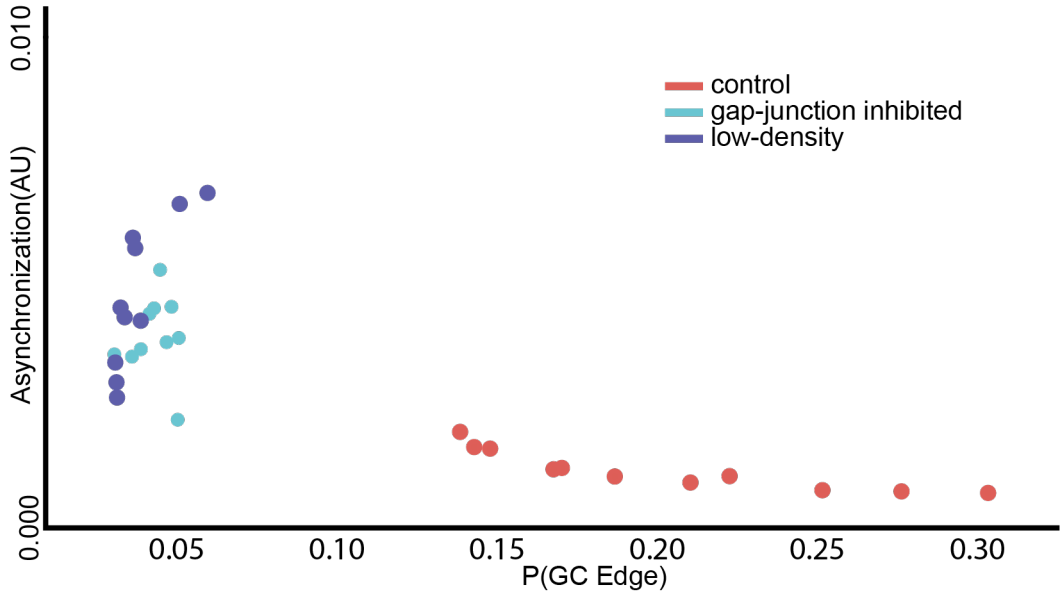

Figure S6: Asynchronization and GC edge probability. Control, representative of 10 experiments (red): asynchronization was negatively associated with GC edge probability (Pearson correlation = -0.8933, p-value ≤ 0.000091). Gap-junction inhibition, representative of two experiments (cyan): asynchronization is not associated with GC edge probability (Pearson correlation = 0.0077, p-value = 0.9829). Low density, representative of two experiments (purple): asynchronization is positively associated (i.e., cells are not synchronizing over time) with GC edge probability (Pearson correlation = 0.8151, p-value = 0.0040). This analysis considered 12 (control), 10 (gap-junction inhibition), 10 (low density) cycles. The first cycle was an outlier and was excluded from this analysis.

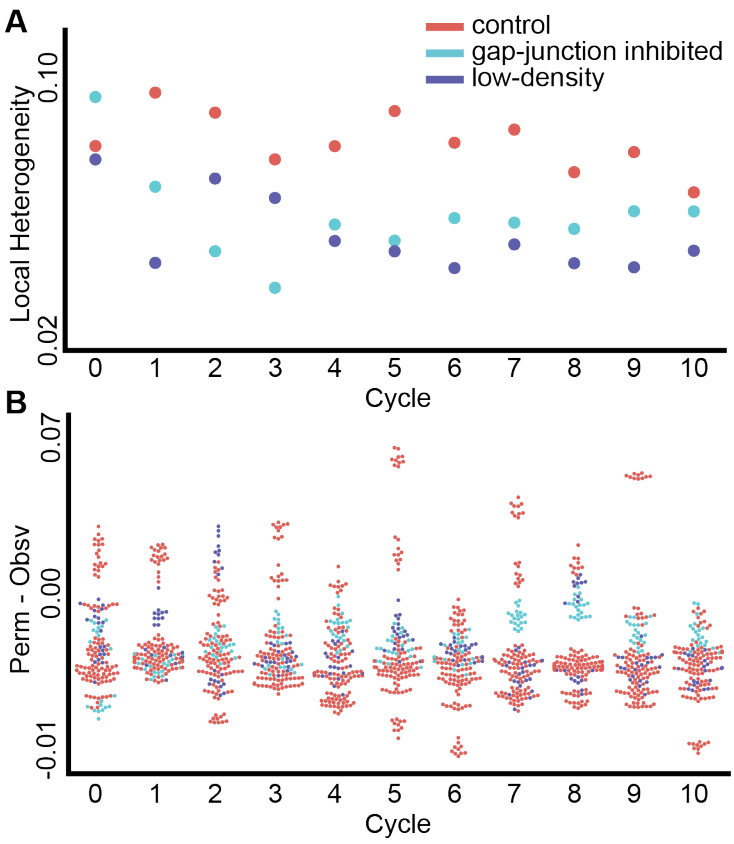

Figure S7: Local heterogeneity over time
(**A**) Control experiment, representative of ten experiments (red) (Pearson correlation = -0.6127, p-value = 0.0450), gap junction inhibition experiment, representative of two experiments (Pearson correlation = -0.2973, p-value = 0.3744) (cyan) and low density experiment, representative of two experiments (purple) (Pearson correlation = -0.6688, p-value = 0.0244).
(**B**) Each point represents the difference between a single permutation of the null model that spatially shuffles the cells' neighbors while preserving the same degree rank and the observed experiment for local heterogeneity (see Methods) over all the cycle experiments replication. Control experiments (red, n=10). Gap junction inhibition experiments (cyan, n=2). Low density experiments (purple, n=2). There is no clear separation between the control, gap-junction inhibited, and low-density experiments.

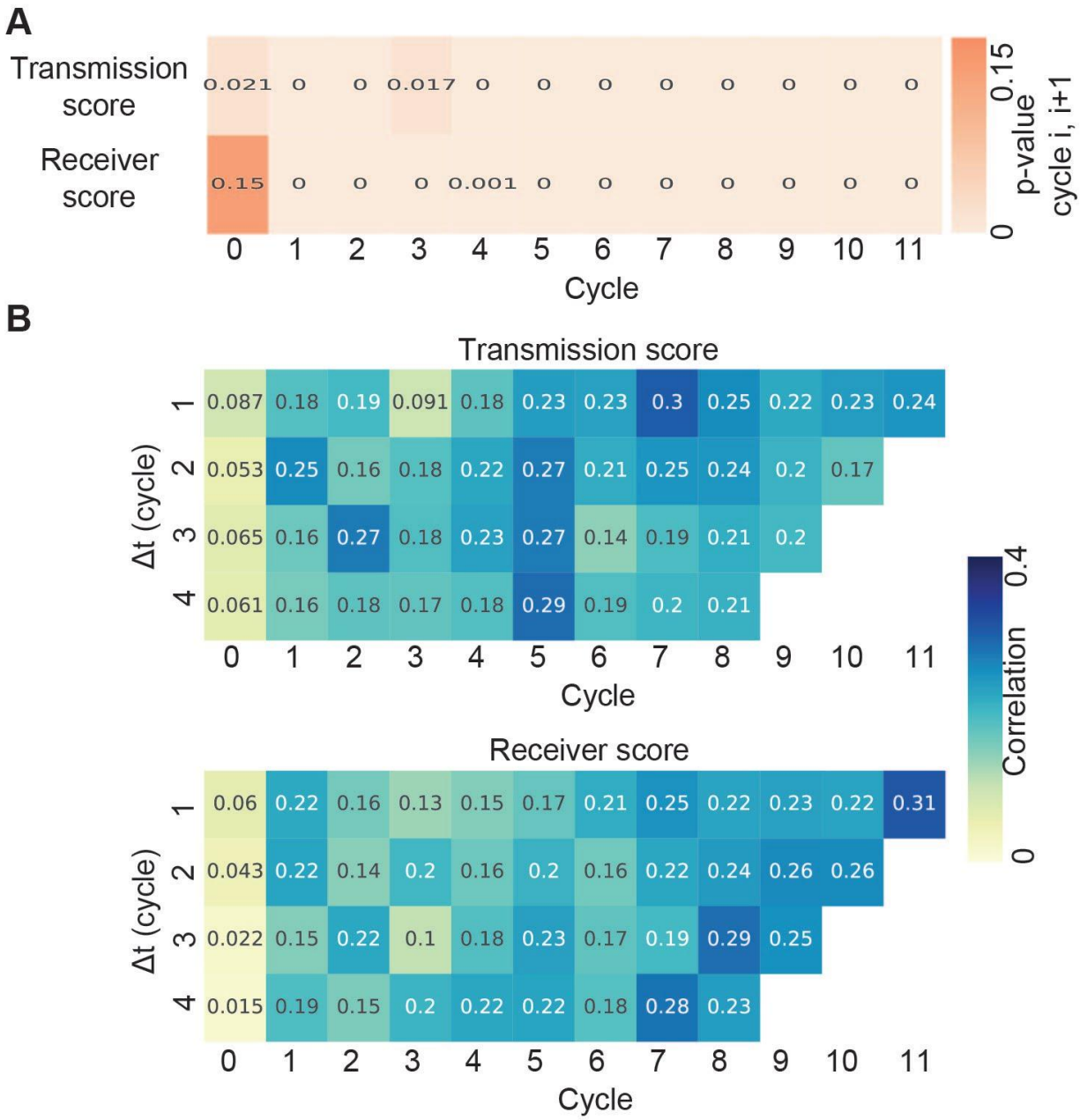

Figure S8: Single cell communication memory. Representative of ten control experiments.
(**A**) P-value of the correlation between the cells' transmission/receiver scores over consecutive cycles (x-axis), values correspond to the correlations in Fig 4A. The color scale is linear.
(**B**) Longer term memory. The temporal correlations between single cells' transmission (top) or receiver (bottom) scores with time gaps of 1-4 cycles (y-axis). The x-axis indicate time (cycle #) and the y-axis indicates the number of cycles considered when calculating the correlation. The color scale is linear.

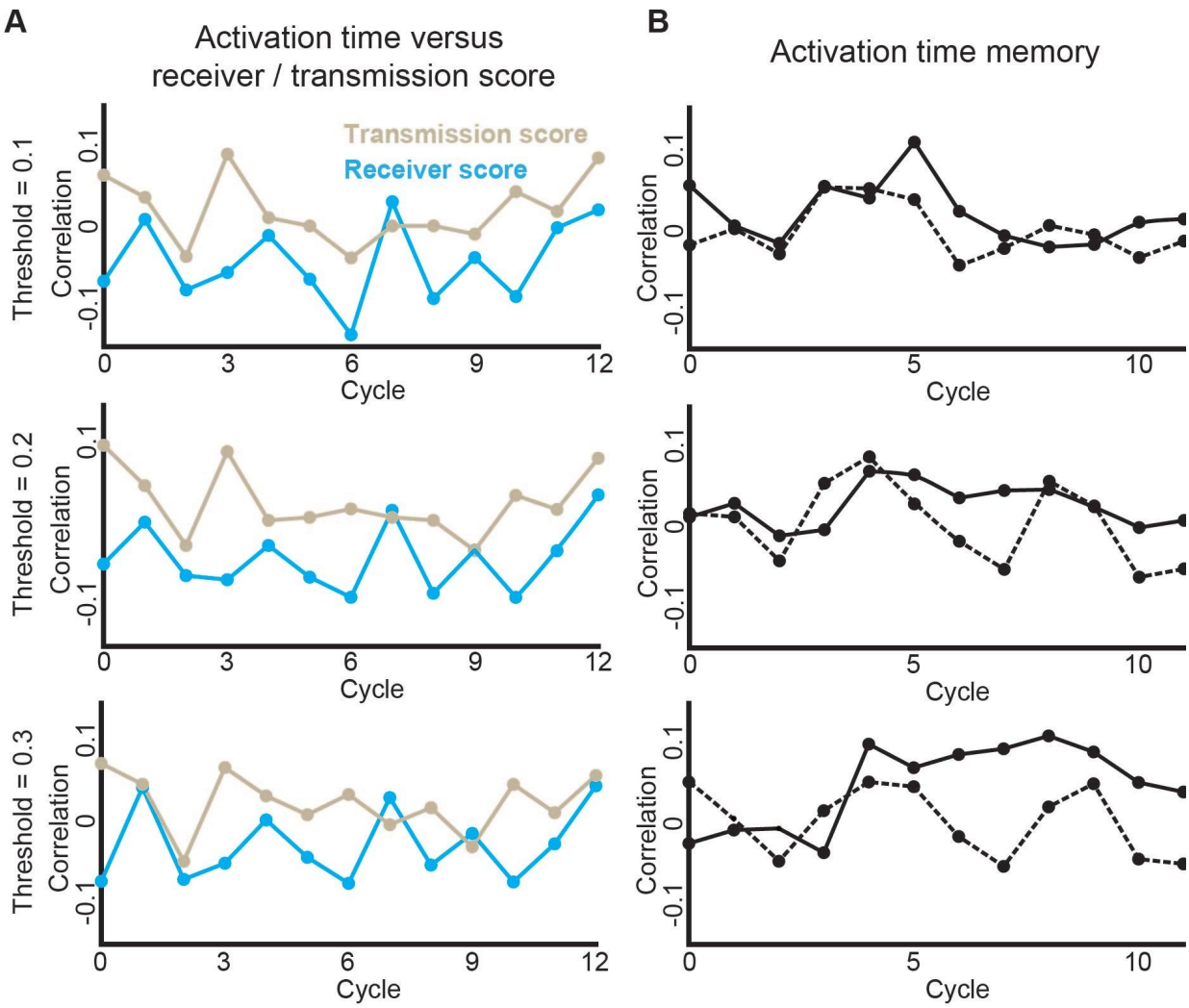

Figure S9: Single cell activation time. Representative of ten control experiments. A cell's activation time was defined as the time where the cell's calcium dynamics exceed δ= 0.1-0.3 (top-to-bottom) from it's maximal signal, see Methods for full details.
(A) Cells' activation time was not correlated with the transmission or the receiver score.
(B) Cells' activation time was not correlated across consecutive cycles (solid lines). The dashed lines were the calculated correlation after shuffling the cells in the next cycle.

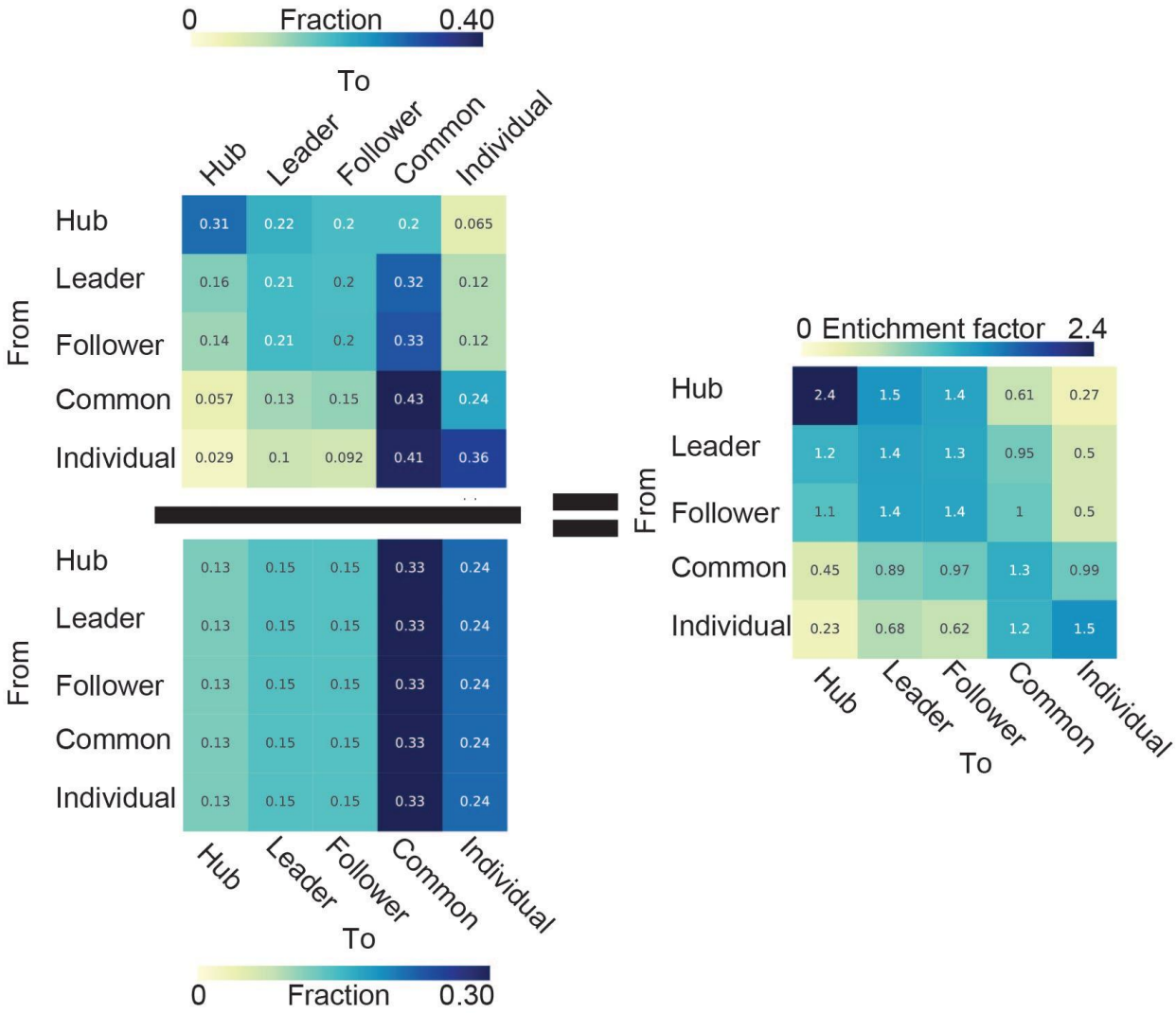

Figure S10: Calculating the enrichment factor of cellular state transitions. Representative of ten control experiments. Top left: Markov transition matrix based on the observed single cell role transition over the cycles. Bottom left: The expected transition probability between two roles based on the cells' roles frequency over the cycles. Right: The enrichment transition matrix was followed by normalizing (scalar division) the Markov transition matrix with the expected transition matrix. The enrichment factor from hub to hub is higher than any other enrichment factor. (see only transitions above the expected, Fig. 5D). The color scale is linear.

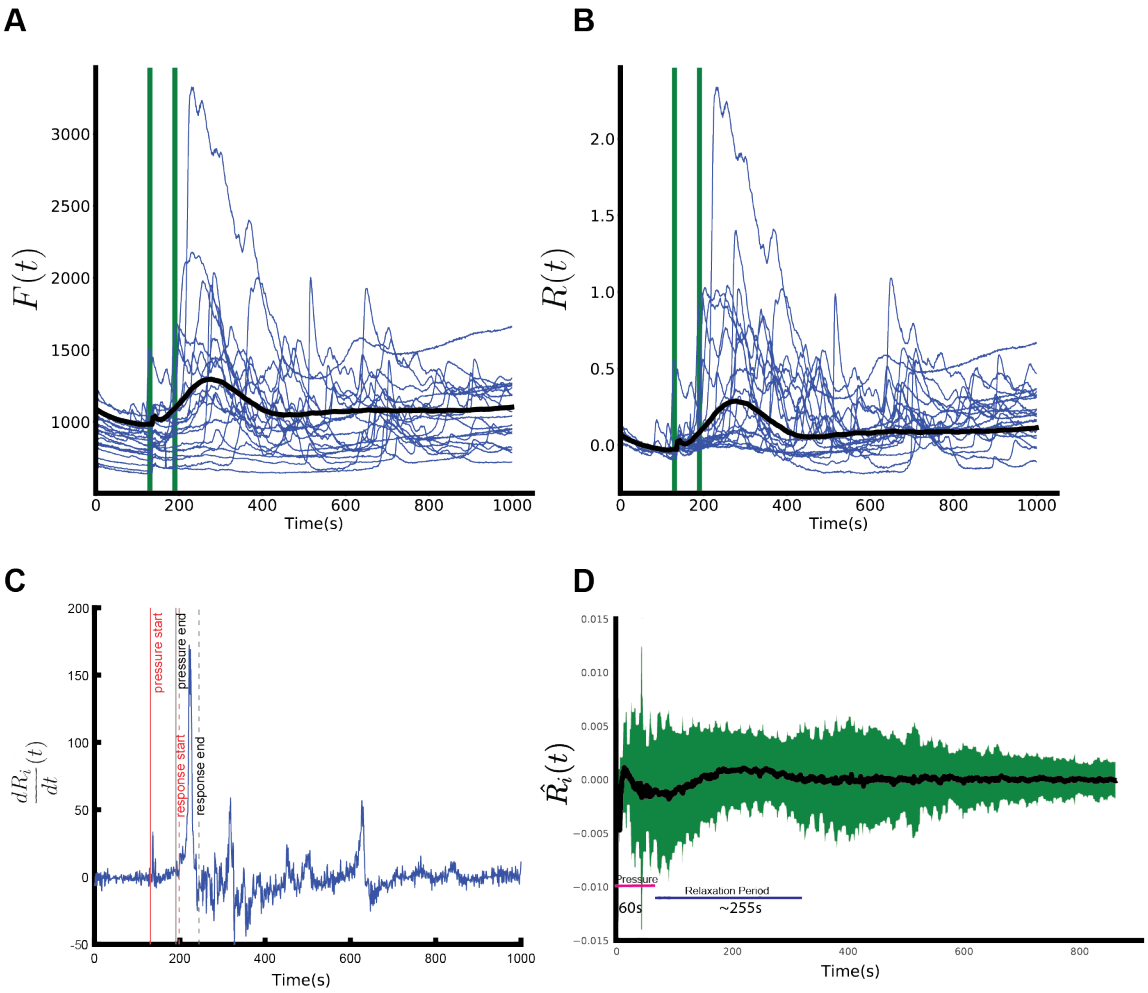

Figure S11: Analysis of stimulation onset and relaxation time after a single pulse of shear stress. Representative of two experiments. To assess single cell relaxation time we performed a new experiment (2 replicates) where, after 130 seconds without stimulation, we applied a pulse of shear stress (0.2 Pa) for 60 seconds and then released the stress and followed the relaxation.
(**A-B**) The raw (A) and normalized (B) calcium intensity time-profile of 20 randomly selected responding cells. For each cell, the calcium peak near the time to the pulse of shear stress application and the time where the cell settled (or "relaxed") were manually annotated. Black: mean intensity. Green vertical line marks the time of the stimuli onset and stop. Single cells reached a steady state ~70-110 seconds after their peak (mean 72.25 seconds, standard deviation 25.3 seconds) and full collective relaxation was achieved after approximately 285 seconds. The fluorescent intensity usually did not return to the pre-stimuli level, but the cells settled to a new basal level that is slightly higher than the original, and do not show changes in the intensity beyond short noise fluctuations (in fact, this is one of our reasons to analyze the temporal derivatives).
(C) Derivative of the normalized calcium intensity of a representative cell. The red solid line indicates the beginning of the pulse and the red dashed line the end of the pulse. The black solid line indicates the start of the manually annotated cell's response and black dashed line the cell's relaxation time.
(D) Multicellular calcium dynamics (black - mean calcium dynamics, green - standard deviation). The 60s of shear stress application is marked in red and the relaxation time is marked in blue.

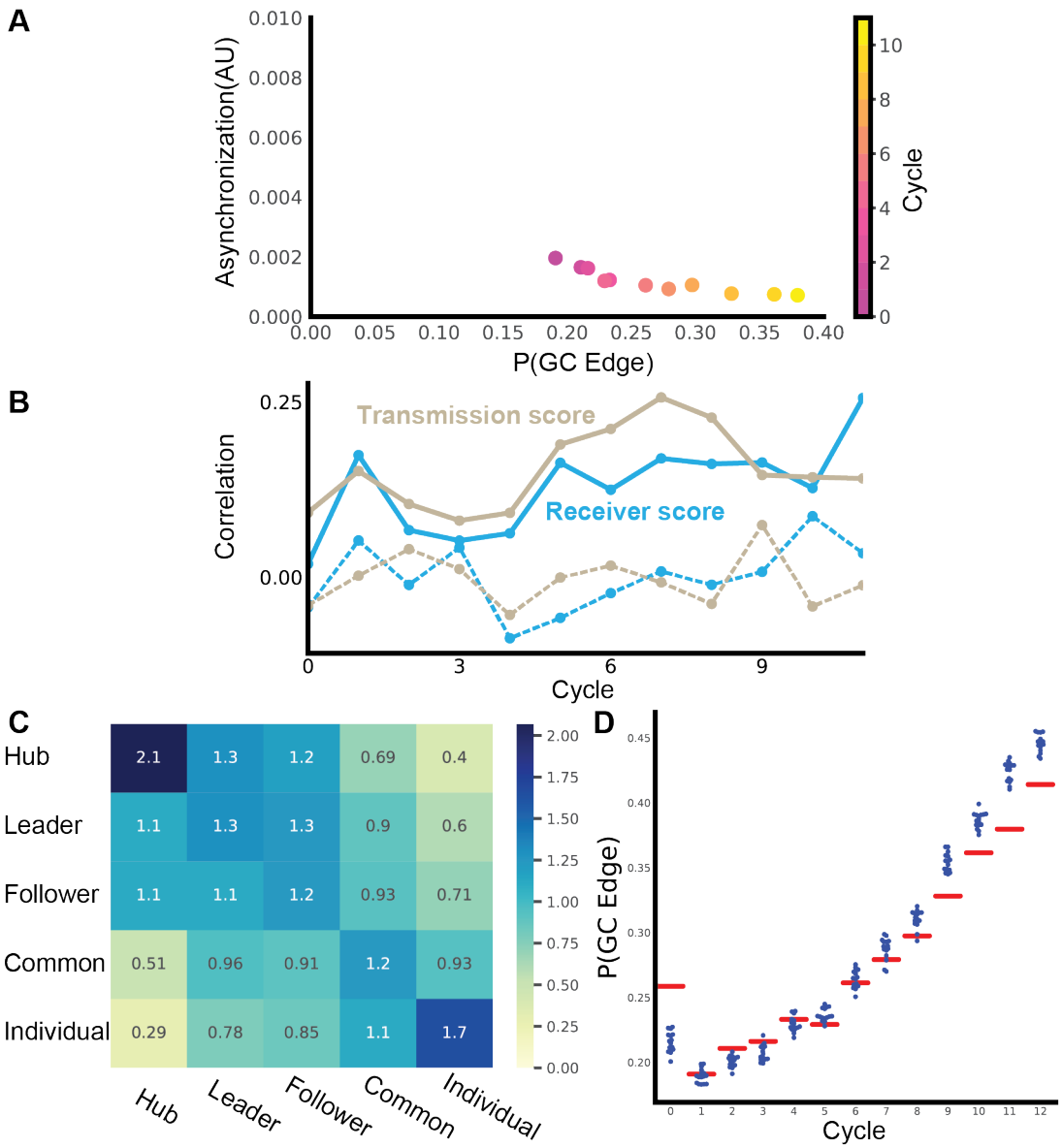

Figure S12: Replication of main results with topological distance of one. Representative of ten control experiments.
(A) Asynchronization was negatively associated with GC edge probability (Pearson correlation = -0.8972, p-value = 0.0002). The first cycle was an outlier and was excluded from this analysis. The color scale is linear.
(B) Cells transmission and receiver scores were correlated across consecutive cycles (solid lines), reinforced over time (Pearson coefficient = 0.5620, $p < 0.0044$), and were a local cell property as validated with permutation analysis – shuffling the cells in the next cycle and calculating correlation (dashed line, see Methods).
(C) The enrichment transition matrix**.** The enrichment factor from hub to hub is higher than any other enrichment factor. The color scale is linear.
(D) Gradual local to global transition in information spreading. The observed versus permuted Granger causality edge probability, P(GC edge), over the cycles. The red horizontal line is the experimental observation, while each blue dot is the result of one of ten independent spatial cell permutations.

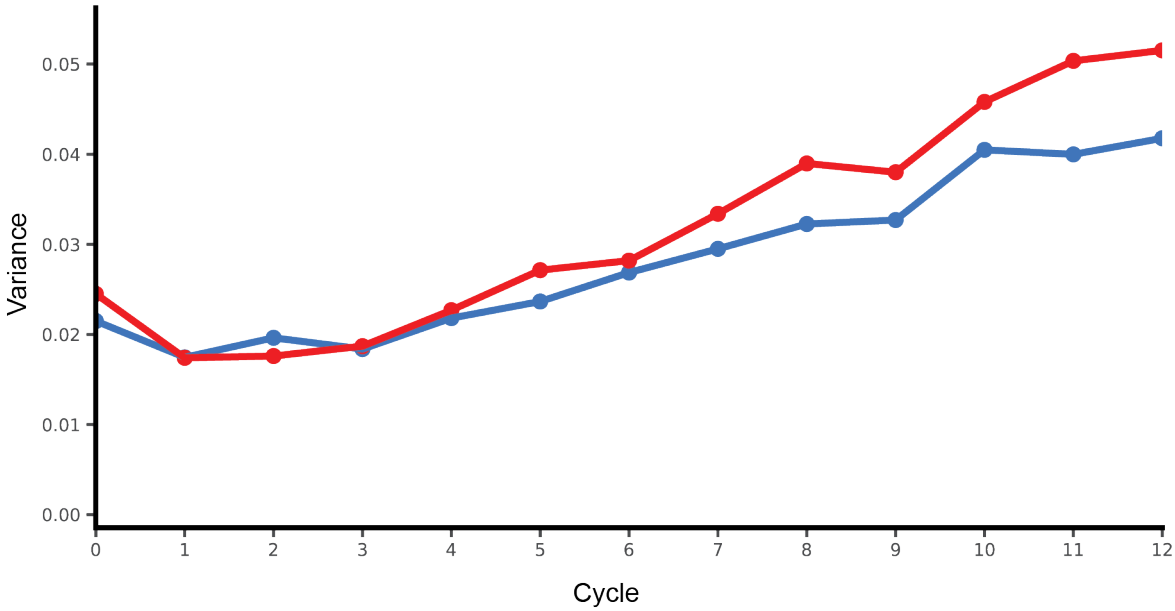

Figure S13: Variance in the cells' raw (i.e., before normalization) transmission (red) and receiver (blue) scores for each cycle. Representative of ten control experiments. The variance is increased over time in the transmission score (Pearson coefficient = 0.9541, $p < 0.0001$) and in the receiver score (Pearson coefficient = 0.9442, $p < 0.0001$).

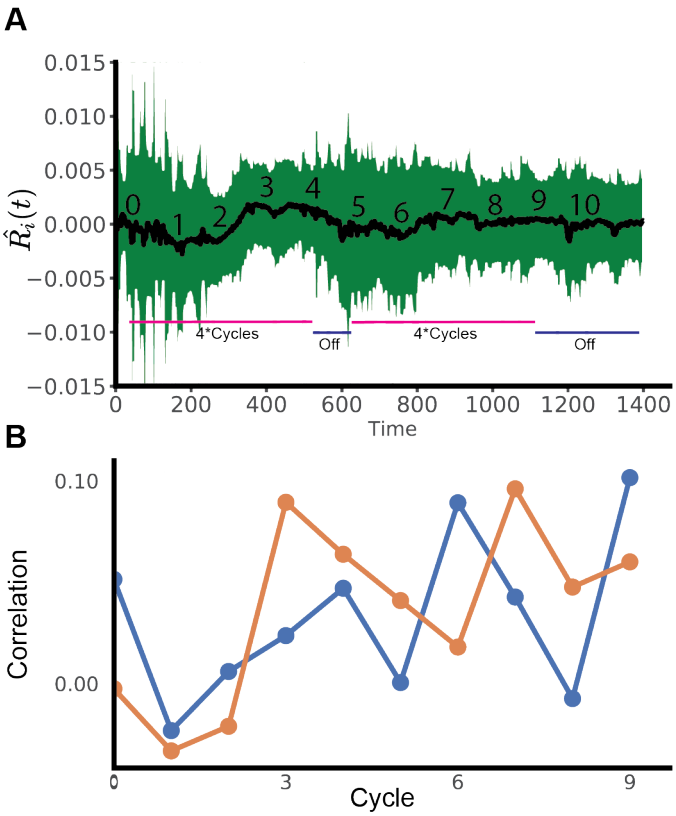

Figure S14: Cycle experiment were the shear stress was turned off for one cycle (cycle #4) showed weak memory.

(A) Multicellular calcium dynamic. Black indicates the mean calcium dynamics, and green the standard deviation. Numbers indicate periodic shear stress cycles, horizontal pink lines mark rounds of 4 consecutive cycles, and horizontal blue lines marks times were the shear stress was turned off.
(**B**) Cells transmission and receiver scores were marginally but positively correlated across consecutive cycles (solid lines), and slightly increased over time (Pearson coefficient = 0.6092, $p < 0.0616$). Shown are correlations with time delay of two cycles. This specifically included the positive correlation at cycle #3 (x-axis, between cycle 3 and 5) that involved the “idle” (i.e., no shear stress application) cycle.